Kovachy Group simulation tools for studying laser aberrations

Natasha Sachdeva

Laser wavefront aberrations

- A key challenge is prevention of dephasing of the atoms due to laser wavefront aberrations
- Laser *intensity* perturbations lead to phase shifts through light shifts (intensity dependent phase shifts)
- The laser *phase* profile is imprinted on the atom when photons are absorbed or emitted
- Target value for laser wavefront variation: 5 mrad at transverse length scales less than 3 mm

Intensity ripples change with height (diffraction)

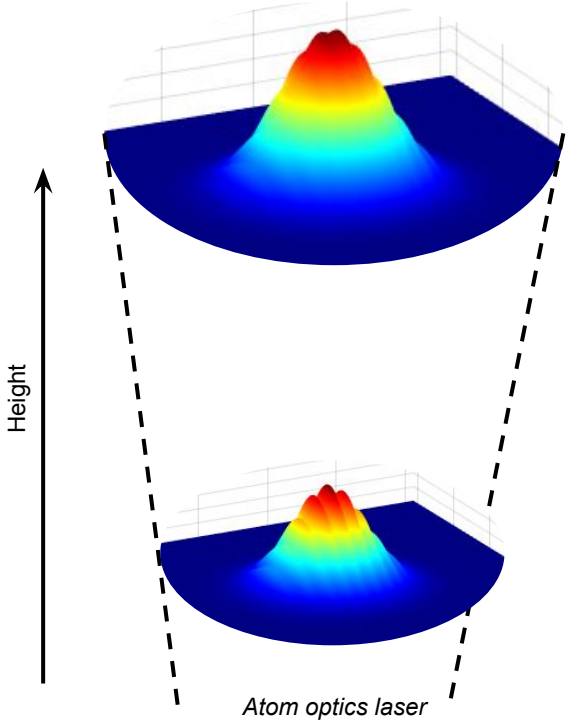

FFT Beam Propagation in Matlab

Two FFT-based propagation methods that use full Rayleigh-Sommerfeld diffraction (RSD) integral—no approximations

$$U(x',y',z') = \frac{1}{2\pi}\iint_A U(x,y,0)\frac{e^{-ikr}}{r}\frac{z'}{r}\left(ik+\frac{1}{r}\right)dx\,dy$$

1. Angular spectrum method (short distances only)
2. Evaluation of RSD using FFT convolution theorem*

Code speedup realized through parallelization with CUDA-enabled graphics card

- With GPU utilization, propagation of 4096x4096 array typically runs in about 5 seconds

*F. Shen and A. Wang, Appl. Opt. 45, 1102-1110 (2006)

Diffraction from dust particle, comparison with analytical form

Blue : analytic
Orange : simulation

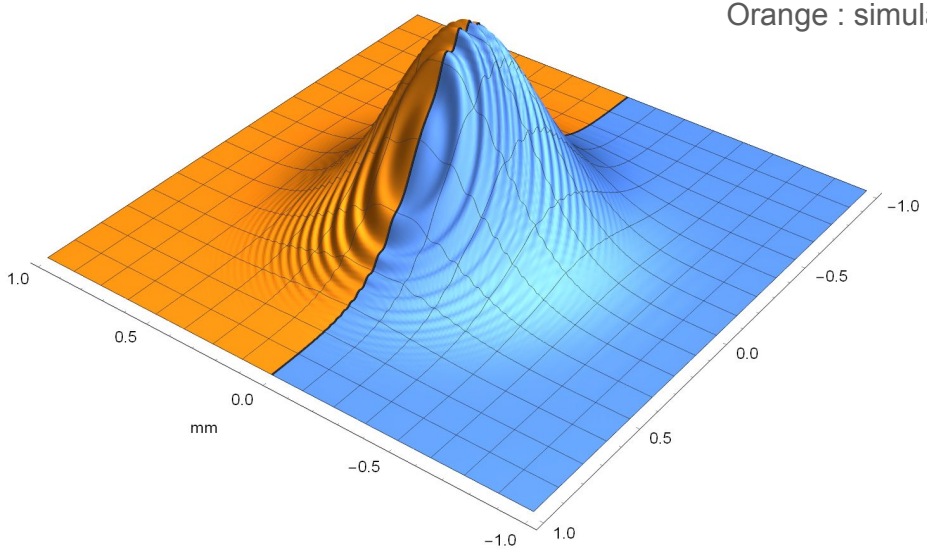

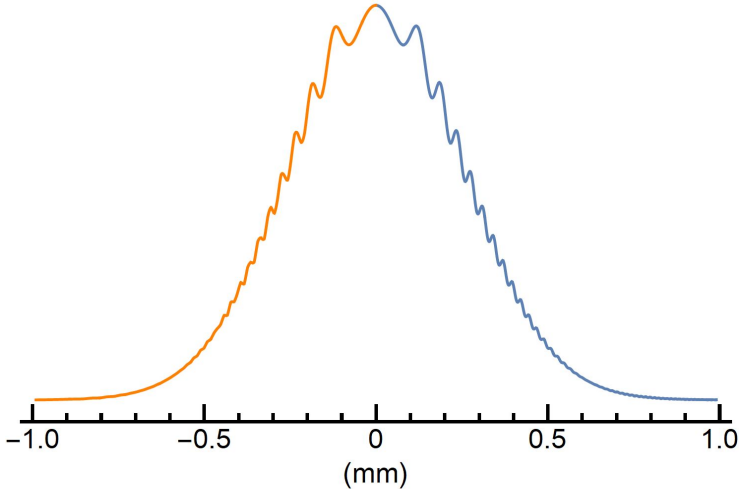

Top: Cross section of Gaussian beam profile after incidence with a dust particle on the propagation axis

Left: Gaussian Beam profile after incidence with an off-axis dust particle

See “Beam Propagation with Aberrations” on doc.db for more on benchmarking

Beam propagation studies for the MAGIS-100 telescope (2-lens vs 3-lens studies)

Intensities for 2-lens for various tilts

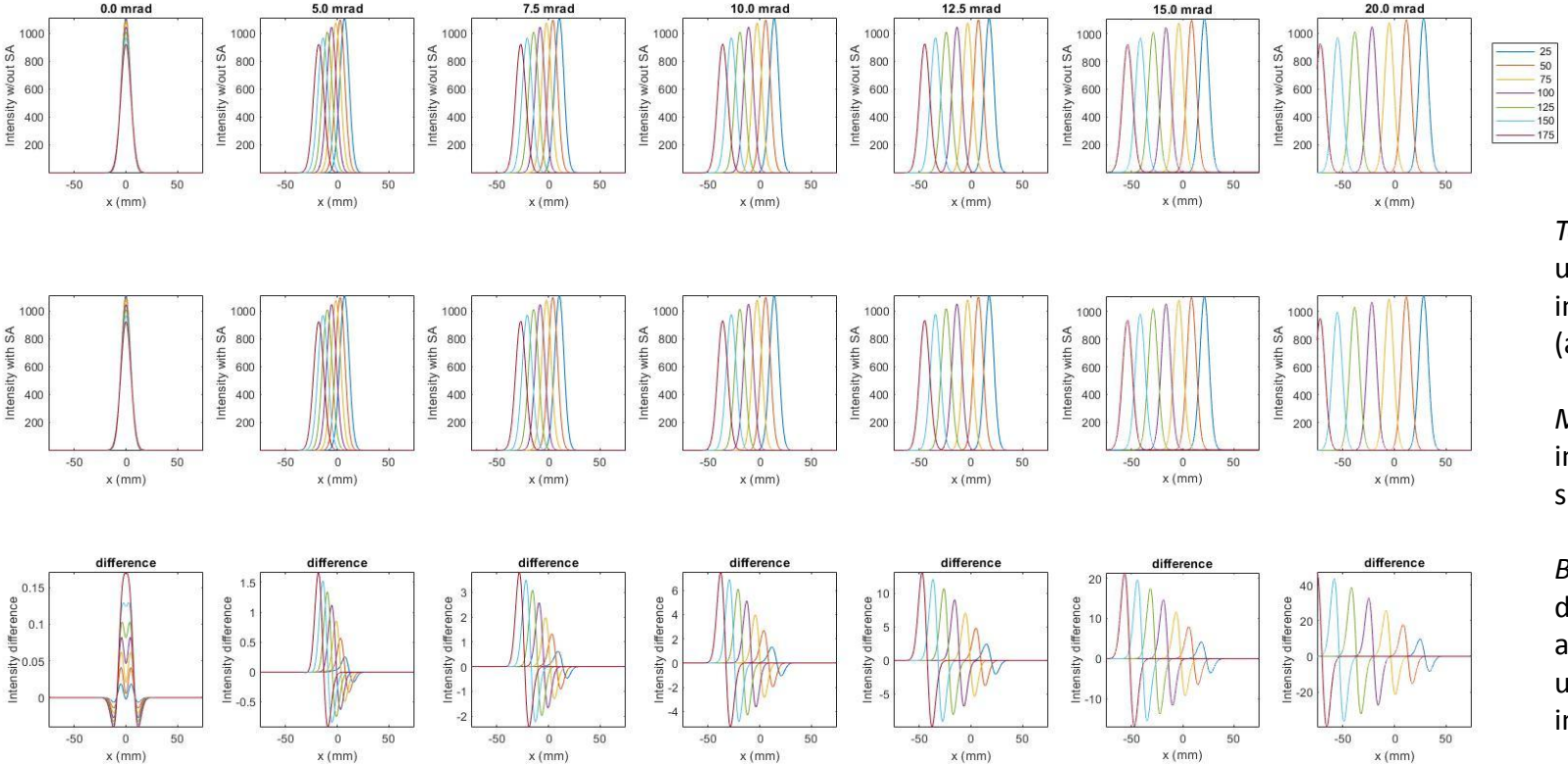

Top row: unaberrated intensity (arbitrary units)

Middle row: intensity with spherical lenses

Bottom row: difference of aberrated and unaberrated intensities

See “Aberrations of the MAGIS-100 Magnifying Telescope” on doc.db for more on the 2-lens vs 3-lens telescope studies

MAGIS-100 Pre-vacuum telescope

- The pre-vacuum telescope focuses the beam down to 300 μm over 4 m before the 1:30 magnifying telescope
- Perturbations of different spatial frequency diffract out at different rates
- MAGIS-100 is most sensitive to wavefront perturbations with spatial scale <3 mm
- Bottom row shows sidepeaks diffracting out over distance

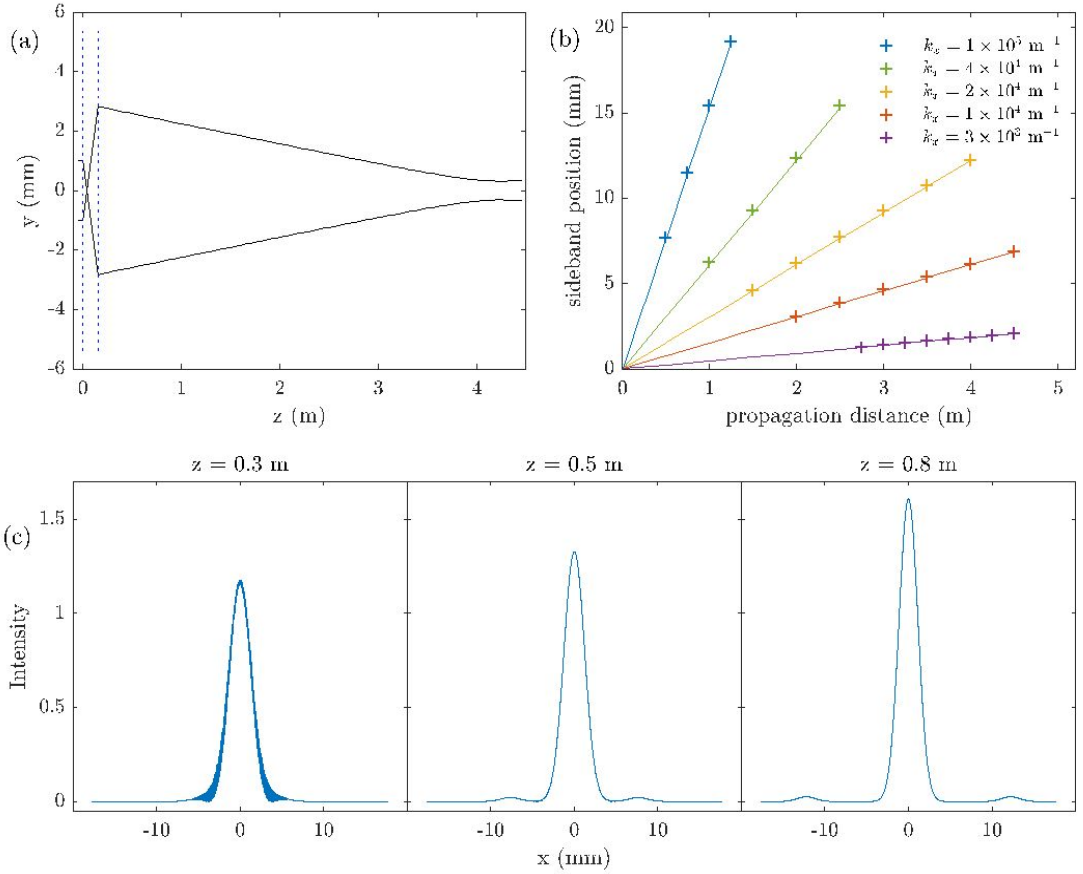

Spatial mode cleaning via free space propagation before telescope

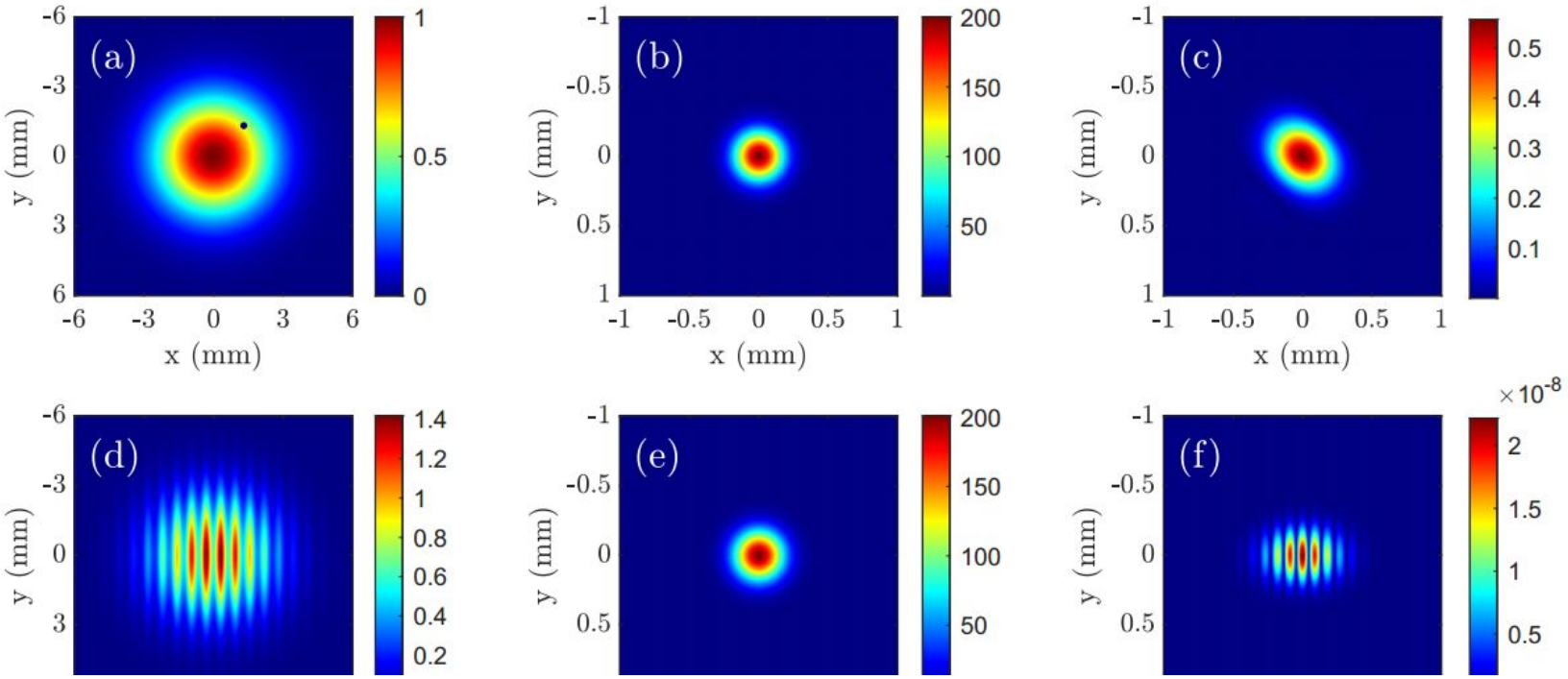

Spherical aberrations in MAGIS-100 telescope

Ideal lens: parabolic

$$\Delta = -k \times \frac{r^2}{2f}$$

Real lens: spherical

$$\Delta = -k \times (\frac{r^2}{2f} + \frac{r^4}{2f^3})$$

The spherical aberration on the beam profile at the reflecting mirror (100 m after the telescope).

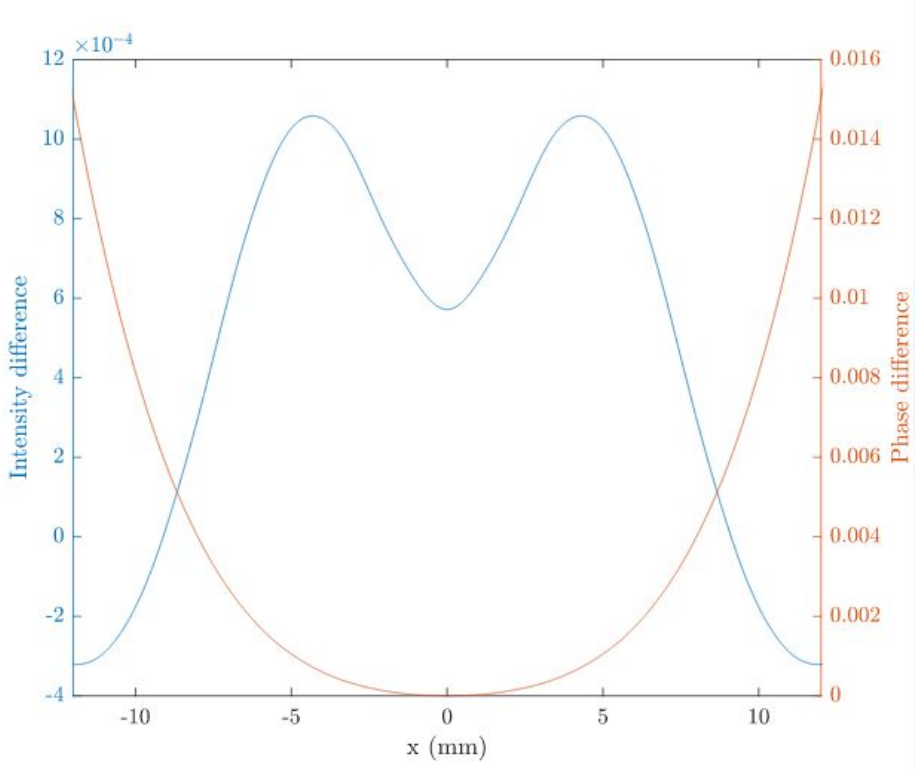

Path integral approach to final phase calculation

- Follows standard semi-classical approach
- Assign phases to classical trajectories
- Calculating phase along interferometer trajectories using input initial position and velocity
- Recently implemented LMT/finite pulses
- Truncation errors may be an issue with double precision depending on the application, can use multiprecision toolbox in Matlab for arbitrary precisior. but it is slow
- Looking into using native quadruple precision in Fortran or C++

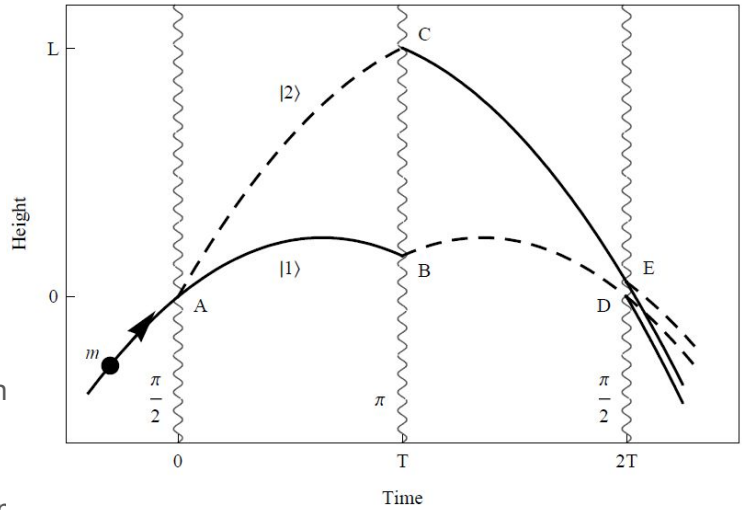

$$\Delta\phi_{\text{prop}} = \frac{1}{\hbar}\int_{\text{upper path}} \mathcal{L} - \frac{1}{\hbar}\int_{\text{lower path}} \mathcal{L}$$

$$\Delta\phi_{\text{laser}} = \sum_i \phi_{\text{imprint}}\left(\mathbf{r}_i^{\text{upper}}\right) - \sum_i \phi_{\text{imprint}}\left(\mathbf{r}_i^{\text{lower}}\right)$$

$$\Delta\phi_{\text{sep}} = \frac{1}{\hbar}\overline{\mathbf{p}}_{\text{final}} \cdot \Delta\mathbf{r}_{\text{final}}$$

https://arxiv.org/abs/0806.3261

$$\Delta\phi = \Delta\phi_{\text{prop}} + \Delta\phi_{\text{laser}} + \Delta\phi_{\text{sep}}$$

	Phase shift	Size (rad)	Fractional size
1	$-k_{\text{eff}} g T^2$	-2.85×10^{8}	1.00
2	$k_{\text{eff}} R_e \Omega_y^2 T^2$	6.18×10^{5}	2.17×10^{-3}
3	$-k_{\text{eff}} T_{zz} v_z T^3$	1.58×10^{3}	5.54×10^{-6}
4	$\frac{7}{12} k_{\text{eff}} g T_{zz} T^4$	-9.21×10^{2}	3.23×10^{-6}
5	$-3 k_{\text{eff}} v_z \Omega_y^2 T^3$	-5.14	1.80×10^{-8}
6	$2 k_{\text{eff}} v_x \Omega_y T^2$	3.35	1.18×10^{-8}
7	$\frac{7}{4} k_{\text{eff}} g \Omega_y^2 T^4$	3.00	1.05×10^{-8}
8	$-\frac{7}{12} k_{\text{eff}} R_e T_{zz} \Omega_y^2 T^4$	2.00	7.01×10^{-9}
9	$-\frac{\hbar k_{\text{eff}}^2}{2m} T_{zz} T^3$	7.05×10^{-1}	2.48×10^{-9}
10	$\frac{3}{4} k_{\text{eff}} g Q_{zzz} v_z T^5$	9.84×10^{-3}	3.46×10^{-11}
11	$-\frac{7}{12} k_{\text{eff}} Q_{zzz} v_z^2 T^4$	-7.66×10^{-3}	2.69×10^{-11}
12	$-\frac{7}{4} k_{\text{eff}} R_e \Omega_y^4 T^4$	-6.50×10^{-3}	2.28×10^{-11}
13	$-\frac{7}{4} k_{\text{eff}} R_e \Omega_y^2 \Omega_z^2 T^4$	-3.81×10^{-3}	1.34×10^{-11}
14	$-\frac{31}{120} k_{\text{eff}} g^2 Q_{zzz} T^6$	-3.39×10^{-3}	1.19×10^{-11}
15	$-\frac{3\hbar k_{\text{eff}}^2}{2m} \Omega_y^2 T^3$	-2.30×10^{-3}	8.06×10^{-12}
16	$\frac{1}{4} k_{\text{eff}} T_{zz}^2 v_z T^5$	2.19×10^{-3}	7.68×10^{-12}
17	$-\frac{31}{360} k_{\text{eff}} g T_{zz}^2 T^6$	-7.53×10^{-4}	2.65×10^{-12}
18	$3 k_{\text{eff}} v_y \Omega_y \Omega_z T^3$	2.98×10^{-4}	1.05×10^{-12}
19	$-k_{\text{eff}} \Omega_y \Omega_z y_0 T^2$	-7.41×10^{-5}	2.60×10^{-13}
20	$-\frac{3}{4} k_{\text{eff}} R_e Q_{zzz} v_z \Omega_y^2 T^5$	-2.14×10^{-5}	7.50×10^{-14}
21	$\frac{31}{60} k_{\text{eff}} g R_e Q_{zzz} \Omega_y^2 T^6$	1.47×10^{-5}	5.17×10^{-14}
22	$\frac{5}{2} k_{\text{eff}} T_{zz} v_z \Omega_y^2 T^5$	-1.42×10^{-5}	5.00×10^{-14}
23	$-\frac{7}{6} k_{\text{eff}} T_{zz} v_x \Omega_y T^4$	1.08×10^{-5}	3.81×10^{-14}
24	$-2 k_{\text{eff}} T_{xx} \Omega_y x_0 T^3$	-6.92×10^{-6}	2.43×10^{-14}
25	$-\frac{7\hbar k_{\text{eff}}^2}{12m} Q_{zzz} v_z T^4$	-6.84×10^{-6}	2.40×10^{-14}
26	$-\frac{7}{6} k_{\text{eff}} T_{xx} v_x \Omega_y T^4$	-5.42×10^{-6}	1.90×10^{-14}
27	$-\frac{31}{60} k_{\text{eff}} g T_{zz} \Omega_y^2 T^6$	4.90×10^{-6}	1.72×10^{-14}
28	$k_{\text{eff}} T_{xx} v_z \Omega_y^2 T^5$	4.75×10^{-6}	1.67×10^{-14}
29	$\frac{3\hbar k_{\text{eff}}^2}{8m} g Q_{zzz} T^5$	4.40×10^{-6}	1.55×10^{-14}
30	$\frac{31}{360} k_{\text{eff}} R_e T_{zz}^2 \Omega_y^2 T^6$	1.63×10^{-6}	5.74×10^{-15}
31	$-\frac{31}{90} k_{\text{eff}} g T_{xx} \Omega_y^2 T^6$	-1.63×10^{-6}	5.74×10^{-15}
32	$\frac{\hbar k_{\text{eff}}^2}{8m} T_{zz}^2 T^5$	9.78×10^{-7}	3.43×10^{-15}
33	$-\frac{\hbar k_{\text{eff}} \alpha B_0 (\partial_z B) T^2}{m}$	-7.67×10^{-8}	2.69×10^{-16}
34	$\frac{31}{60} k_{\text{eff}} g S_{zzzz} v_z^2 T^6$	-7.52×10^{-8}	2.64×10^{-16}
35	$-\frac{1}{4} k_{\text{eff}} S_{zzzz} v_z^3 T^5$	3.64×10^{-8}	1.28×10^{-16}
36	$\frac{31}{72} k_{\text{eff}} T_{zz} Q_{zzz} v_z^2 T^6$	-3.13×10^{-8}	1.10×10^{-16}

Monte Carlo simulation

- Monte Carlo of initial positions and velocities in three dimensions with provided pdf
- Uses numerical path integral function to get final atom phases at each output port
- Can input a 2D laser phase map from beam propagation simulation
- In Matlab currently but can be interfaced or migrated to Python
- Currently looking into additional parallelization options to make this faster (currently uses multiple CPU cores)

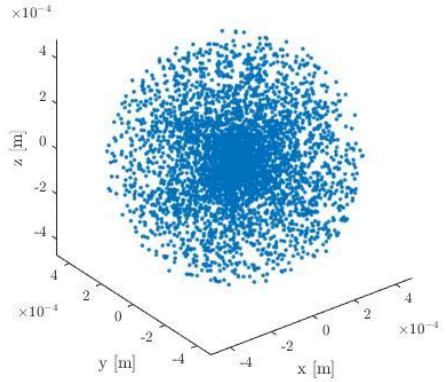

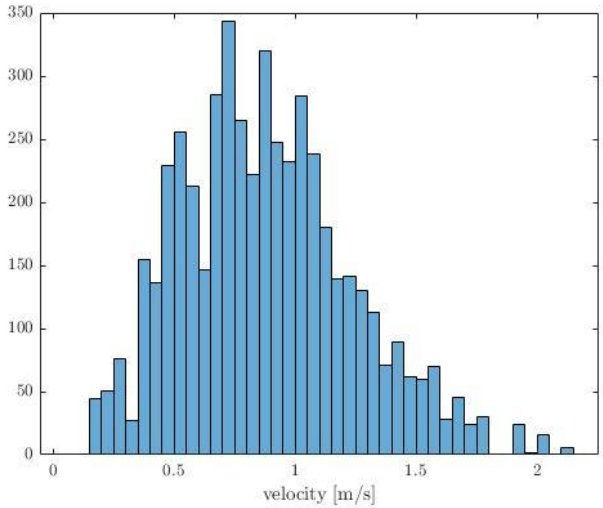

Monte Carlo (point source interferometry example)

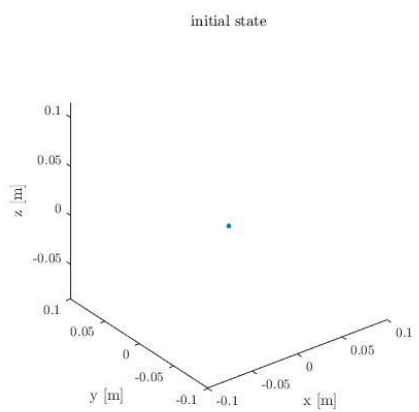

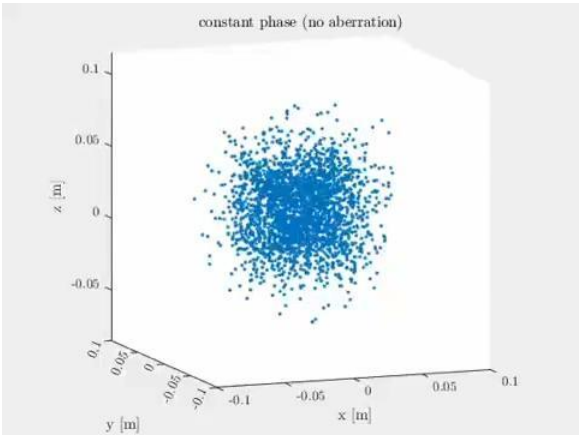

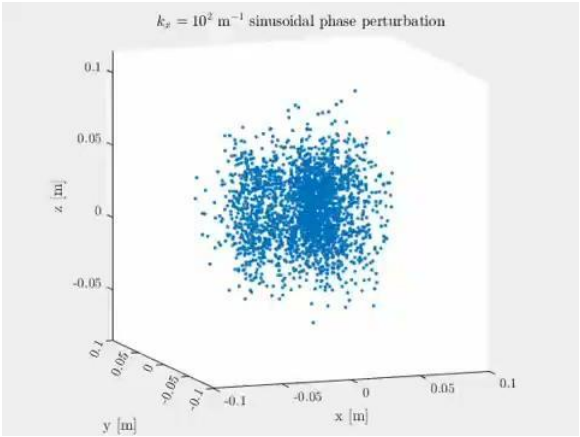

Point source interferometry isolates phase shifts due to laser phase and can be used to measure laser wavefront aberrations

Expansion factor of ~40 shown here

Imaging Process (slide from Yiping Wang)

- Fluorescence imaging for atom cloud after interferometry sequence
- Use Monte Carlo result from previous slide as initial condition
- Use excitation rate to decide if a collision happens, include momentum change and track atom trajectory
- Probability of kick direction

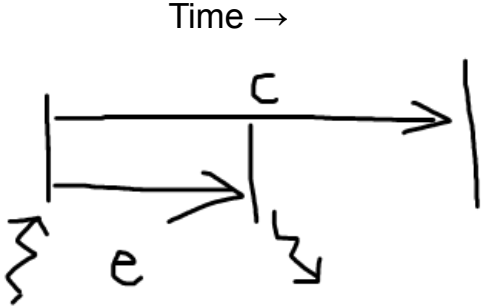

$$\gamma_p = \frac{s_0\gamma/2}{1 + s_0 + \left[2(\delta \pm \omega_D)/\gamma\right]^2}$$

- Track the complete trajectory of each atom throughout the exposure time
- Project final positions to pixels
- Fourier analysis of interference data

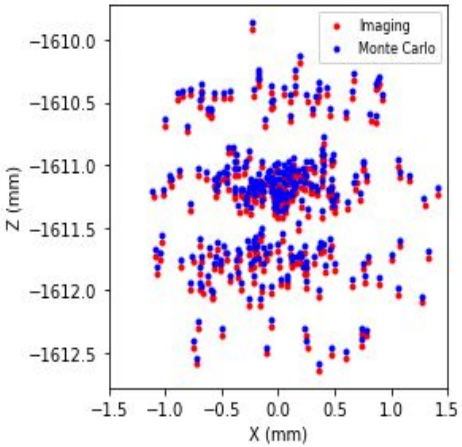

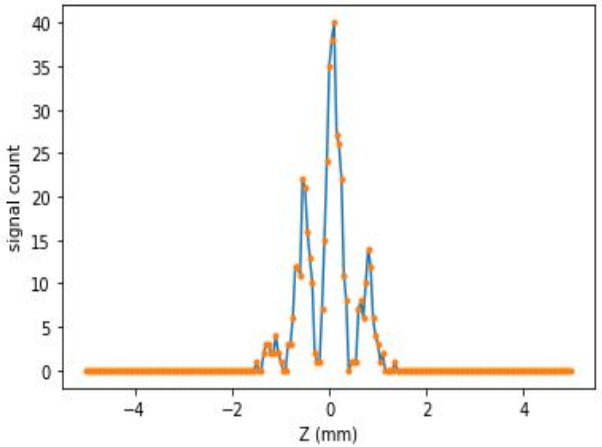

Beam Profiling (slide from Jay Jachinowski)

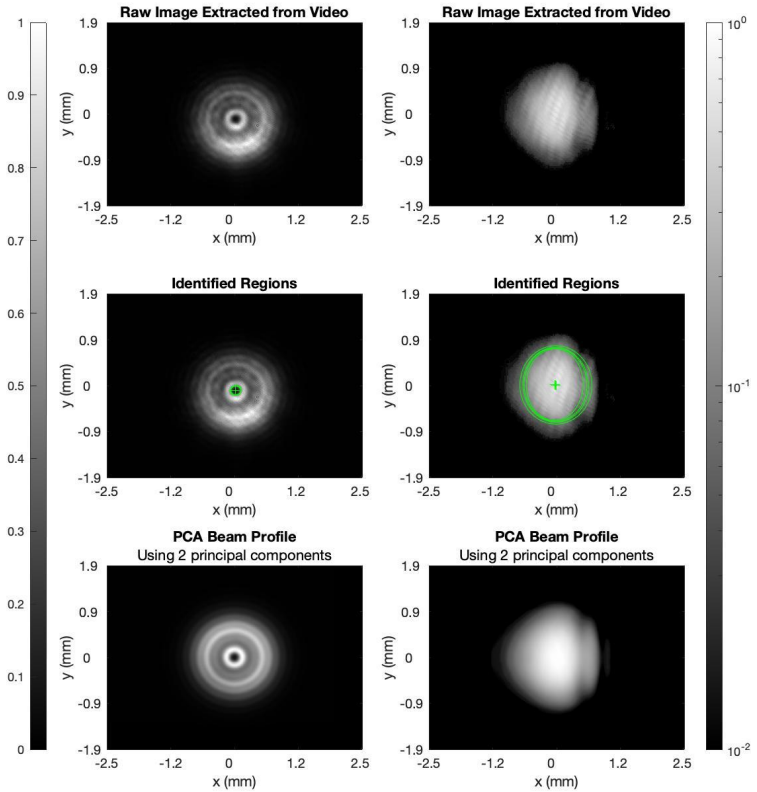

Used camera with CMOS image sensor as a significantly cheaper and faster alternative to CCD image sensor typically used for beam profiling.

Combined video capture, camera translation, computer vision (region detection), and principal component analysis (PCA).

Effectively mitigated fixed pattern noise typical to CMOS image sensors as well as other extraneous noise.

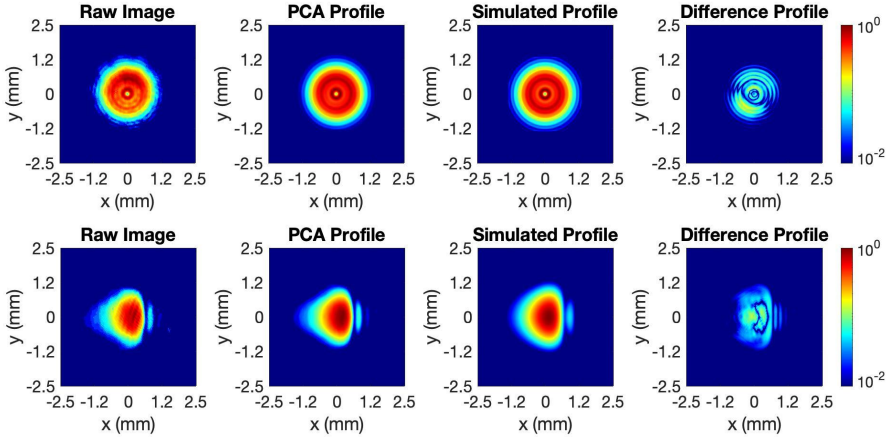

Top: 3.65 mm circular aperture propagating 177 cm. Bottom: hard-edge propagating 229 cm.

Other PCA noise removal algorithms (for single capture)